Remote Sensing of Environment 117 (2012) 236–248

Contents lists available at SciVerse ScienceDirect

Remote Sensing of Environment

journal homepage: www.elsevier.com/locate/rse

Evaluation of passive microwave brightness temperature simulations and snow water equivalent retrievals through a winter season

C. Derksen [a,*], P. Toose [a], J. Lemmetyinen [b], J. Pulliainen [b], A. Langlois [c], N. Rutter [d], M.C. Fuller [e]

[a] Climate Research Division, Environment Canada, Toronto, Canada
[b] Arctic Research Centre, Finnish Meteorological Institute, Helsinki, Finland
[c] Centre d'Applications et de Recherches en Télédétection, Université de Sherbrooke, Québec, Canada
[d] School of the Built and Natural Environment, Northumbria University, Newcastle Upon Tyne, UK
[e] Department of Geography, University of Calgary, Canada

ARTICLE INFO

Article history:
Received 5 July 2011
Received in revised form 30 September 2011
Accepted 30 September 2011
Available online 1 November 2011

Keywords:
Snow water equivalent
Microwave radiometry
Snow emission modeling

ABSTRACT

Plot-scale brightness temperature (T_B) measurements at 6.9, 19, 37, and 89 GHz were acquired in forest, open, and lake environments near Churchill, Manitoba, Canada with mobile sled-based microwave radiometers during the 2009–2010 winter season. Detailed physical snow measurements within the radiometer footprints were made to relate the microwave signatures to the seasonal evolution of the snowpack, and provide inputs for model simulations with the Helsinki University of Technology (HUT) snow emission model. Large differences in depth, density, and grain size were observed between the three land cover types. Plot-scale simulations with the HUT model showed a wide range in simulation accuracy between sites and frequencies. In general, model performance degraded when the effective grain size exceeded 2 mm and/or there was an ice lens present in the pack. HUT model performance improved when simulations were run regionally at the satellite scale (using three proportional land cover tiles: open, forest, and lake) and compared to Advanced Microwave Scanning Radiometer (AMSR-E) measurements. Root mean square error (RMSE) values ranged from approximately 4 to 16 K depending on the frequency, polarization, and land cover composition of the grid cell. Snow water equivalent (SWE) retrievals produced using forward T_B simulations with the HUT model in combination with AMSR-E measurements produced RMSE values below 25 mm for the intensive study area. Retrieval errors exceeded 50 mm when the scheme was applied regionally.

1. Introduction

Reliable information on snow cover is needed for monitoring purposes, understanding the global climate system, and for the evaluation of the representation of snow cover and snow cover feedbacks in climate models. While considerable progress has recently been made in determining trends and variability (including quantifying the statistical uncertainty) in snow extent datasets (Brown & Robinson, 2011; Brown et al., 2010) this level of understanding for snow water equivalent (SWE) remains elusive. SWE can be estimated from ground-based snow depth observations (Jonas et al., 2009; Sturm et al., 2010) although these methods are negatively impacted by the sparse spatial coverage of observations particularly in northern regions. Information on SWE can also be obtained by combining observations and models in an analytical framework. For example, the Canadian Meteorological Centre (CMC) produces a daily gridded global snow depth analysis by combining all available snow observations with a simple snow model (Brasnett, 1999), while the National Weather Service produces daily snow information for the United States and parts of southern Canada through a snow analysis system that also combines observations with a snow model (Carroll et al., 2006; Rutter et al., 2008). These analysis systems tend to perform better in observation rich regions, and the point-wise nature of in situ measurements systematically impacts these products. For instance, the CMC analysis has a tendency towards early loss of snow cover in the spring relative to other datasets because of the shallow bias of snow depths reported from observing sites that tend to be located in clearings (Brown et al., 2010).

Satellite passive microwave data are commonly used for the retrieval of SWE (for example, Kelly, 2009) because of a wide swath, all-weather imaging capabilities, multi-frequency response to the presence of snow on land, and a continuous time series that extends back to 1978. The high uncertainty in SWE retrievals at the hemispheric scale, both in terms of systematic and random error (for example, see Armstrong & Brodzik, 2002; Derksen, 2008; Kelly et al., 2003; Koenig & Forster, 2004), continue to limit the use of these datasets. A different approach is the use of theoretical or semi-empirical radiative transfer models for snow cover, coupled with atmospheric and vegetation models, to simulate microwave emission and inversely calculate snow characteristics from satellite measurements (e.g. Pulliainen et al., 1999; Wiesmann & Matzler, 1999). The more complicated models are

* Corresponding author. Tel.: +1 416-739-5804; fax: +1 416-739-5700.
E-mail address: Chris.Derksen@ec.gc.ca (C. Derksen).

0034-4257/$ – see front matter.
doi:10.1016/j.rse.2011.09.021

sensitive to poorly constrained parameters, computationally expensive, and require precise ancillary data in order to give accurate predictions (i.e. Durand et al., 2008). These factors restrict their operational applicability on a global scale.

A new Northern Hemisphere snow water equivalent (SWE) dataset was recently produced by the European Space Agency GlobSnow initiative (see www.globsnow.info), through an assimilation of satellite passive microwave retrievals and snow depth observations from synoptic weather stations, following the method first described by Pulliainen (2006). When assessed with 21 years of snow survey data (over 178 000 samples) from the former Soviet Union, this technique produced SWE retrievals with RMSE values near 33 mm, and a mean bias of approximately 3 mm for cases with ground measured SWE below 150 mm (Takala et al., 2011). This represents reduced uncertainty compared to standalone hemispheric passive microwave brightness temperature (T_B) difference algorithms for which the RMSE can approach 100% of observations (for example, Foster et al., 1997; Kelly et al., 2003).

The GlobSnow retrievals are produced from a SWE inversion algorithm that utilizes forward T_B simulations with the Helsinki University of Technology (HUT) snow emission model (Pulliainen & Hallikainen, 2001; Pulliainen et al., 1999). In order to improve this retrieval scheme, we require a better understanding of the sources of uncertainty in the forward T_B simulations and how this uncertainty impacts the SWE retrievals. A field campaign conducted near Churchill, Manitoba, Canada during the 2009–2010 winter provided the unique opportunity to assess multi-scale forward T_B simulations and SWE retrievals over the course of a complete winter season. In this study, we utilize this dataset to:

1. Assess the ability of the HUT model to simulate T_B at 19 and 37 GHz as compared to plot scale measurements made with ground based microwave radiometers at a network of sites through a complete winter season. Multiple grain size measurement approaches were utilized in the field, providing the opportunity to better understand how the treatment of grain size impacts model performance.
2. Compare T_B simulations at the satellite scale to measurements from the Advanced Microwave Scanning Radiometer (AMSR-E) to gain an improved understanding of model performance at coarse resolution.
3. Perform an assessment of a SWE retrieval scheme based on forward T_B simulations and AMSR-E data (a similar methodology to that employed within the GlobSnow project) for an observation rich region and time period.

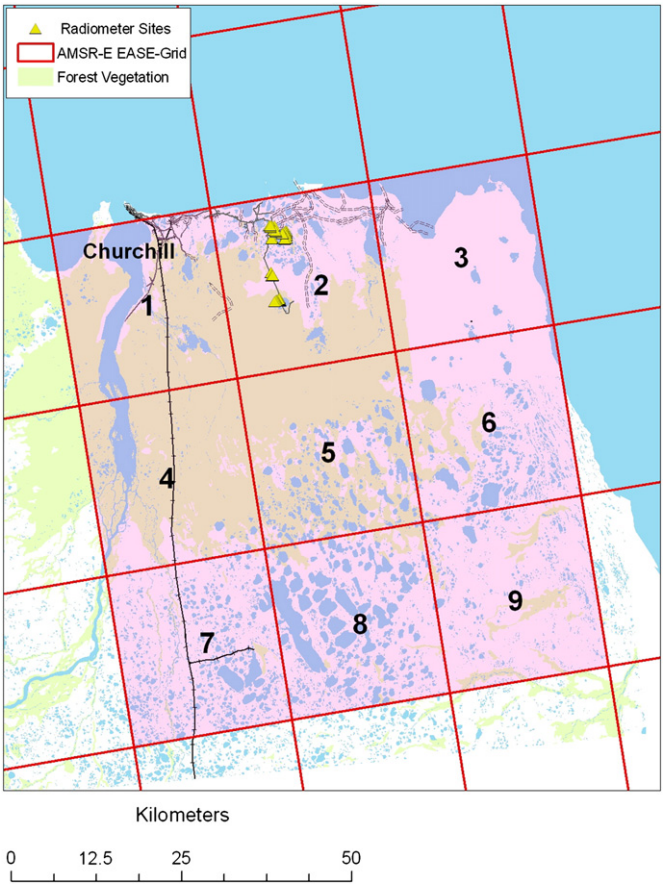

Fig. 1. 3 × 3 EASE-Grid cell study area. Radiometer and snow measurement site are shown within grid cell 2.

2. Data and methods

In order to improve understanding of snowpack metamorphosis over an entire winter, and how these physical changes influence observed T_B, sled-mounted microwave radiometers were deployed near Churchill, Manitoba, Canada between November 2009 and April 2010. During 2 week periods each month, intensive microwave radiometer measurements were acquired at multiple sites in a mixed land cover environment along the forest/tundra transition (Fig. 1). Snowpack observations corresponding to each microwave measurement included snow depth, density, stratigraphy, grain size, and temperature. The mobile nature of the experimental approach allowed radiometer measurements of distinct snowpack types as they evolved through the winter, including deep taiga snow, snow in an open fen, and snow over lake ice. These three sites represent the predominant land cover categories (forest stands, open environments, lakes) found in this region.

The snowpack in mid-November 2009 was shallow (<20 cm) and composed of a single layer. The majority of accumulation occurred in December and January, creating a multi-layered snow cover. Conditions from late January into March were largely cold (−15 to −30 C) and clear, with limited fresh snow accumulation, which drove a period of marked snow metamorphism with dramatic kinetic grain growth. Brief melt events driven by exceptionally warm temperatures in March (nearly 25 °C above normal) produced ice lenses and melt crusts with considerable vertical and horizontal variability. End of season snow melt onset occurred earlier than normal – by mid-April 2010 the snowpack was saturated.

2.1. Radiometer measurements

Sled-mounted microwave radiometers (6.9, 19, 37 and 89 GHz; dual-pol; Fig. 2) were deployed to improve understanding of the impact of seasonal snowpack metamorphosis on measured T_B. The sled system was designed specifically for these instruments, and allowed straightforward access to all measurement sites. Radiometer specifications are provided in Table 1.

An overview of the radiometer sampling periods through the campaign is provided in Table 2 (note that Ku- and X-band scatterometer measurements were also acquired during the campaign, but are not utilized in this study). At each measurement site, the radiometers were incrementally shifted slightly (~75 cm) between a series of three fixed measurement points in order to determine the variability in measured T_B across overlapping footprints. Snowpits were excavated in the middle of the center footprint immediately after the radiometer measurements were completed.

The radiometers were calibrated at regular intervals through each intensive observing period for conversion of voltage output to T_B. A two-point calibration technique was used with an ambient temperature microwave absorber as the 'warm' reference, and liquid nitrogen as the 'cold' reference following the technique described in Solheim (1993). The errors in the measurement of the calibration target

Fig. 2. The Environment Canada sled-based microwave radiometer system in measurement configuration.

Table 1
Specifications of the Environment Canada radiometer system.

Frequency [GHz]	6.9	19	37	89
Manufacturer/Model	Attex Inc.	Radiometrics AC1900	Radiometrics AC3700	Radiometrics AC8900
Bandwidth [MHz]	500	1000	2000	4000
Integration time [s]	1	1	1	1
Sensitivity [K]	0.2	0.04	0.03	0.08
Accuracy [K]	<2	<2	<1	<1
Beam width [°]	9	6	6	6
Incidence angle [°]	53	53	53	53
Footprint size (m; ~1.5 m instrument height)	1×1	0.6×0.6	0.6×0.6	0.6×0.6

temperatures were estimated to be less than 2 K, due to the influence of the liquid nitrogen containment target at the cold point, and uncertainty in the physical temperature measurement of the microwave absorbing material at the warm point.

For each calibration period and target, a stable three minute measurement period was selected. For the 19, 37, and 89 GHz radiometers, such measurements from two consecutive two-point calibrations (typically separated by 2 to 5 days) were then input to a non-linear, iterative procedure (developed by Radiometrics Inc.) which produced the final coefficients for converting the raw measured target, load, and noise diode voltages to T_B. For the 6.9 GHz radiometer, each set of warm and cold point measurements were used to determine the voltage versus T_B relationship for each calibration. Coefficients derived from this linear relationship were utilized to convert measured voltage to T_B.

Calibrations from before and after each measurement were therefore utilized in the processing of the final T_B values for a given measurement. From this procedure, the stability of the radiometers between each calibration period was identified: T_B uncertainty was estimated at each calibration point from the differences between the calculated and theoretical liquid nitrogen measurement (~80 K), and the calculated and measured warm point physical temperature, or the <2° uncertainty in the target temperature, whichever was higher. Table 3 provides the root mean square error (RMSE) for each frequency and polarization at the cold and warm points. RMSE for the 6.9 V measurements was not calculated due to the failure of the vertical channel receiver of this instrument in November. 6.9 V measurements continued to be made for the remainder of the campaign by physically rotating the H-pol antenna.

2.2. Snow measurements

Manual snowpit observations were made at each radiometer measurement site. These observations provided baseline information on the evolving vertical structure of the snowpack through the season. Standard field methods were used to measure snow stratigraphy, density, and SWE (Colbeck et al., 1992). Stratigraphic observations including layer thickness were determined by visual and physical examination of the snowpit face. The minimum, mean, and maximum snow grain axes dimensions in each layer were estimated from manual observations using a stereo-microscope and comparator card. Density profiles were determined with 100 cm^3 cutters. During the November and December measurement periods (see Table 2) manual snowpits following this protocol were performed within the radiometer footprints at the disturbed sites.

From January onwards, an enhanced snowpit sampling protocol was employed within the radiometer footprints. Within this enhanced protocol, approximately 20 snow grains were extracted at 5 cm vertical increments and photographed using a directional lighting system whereby the grains were deposited onto a snow pit card and a successive sequence of photos were taken using a single LED illumination source from the four cardinal directions. Digitization of the resulting grain shadows was used to quantify grain dimension (short/long axis, projected surface, and eccentricity) and other characteristics including

Table 2
Overview of campaign schedule and activities. For a description of manual versus enhanced snowpits, see Section 2.2.

Campaign period	Date	Radiometer	Scatterometer	Manual snowpits	Enhanced snowpits	Snow surveys
IOP1[a]	11–26 November 2009	Roving	Roving	Yes	No	Yes
EP1[b]	27 November–18 December 2009	Roving	Fixed	Yes	No	Yes
IOP2	7–15 January 2010	Roving	Roving	Yes	Yes	Yes
EP2	16 January–8 February 2010	No	Fixed	Yes	No	Yes
IOP3	9–18 February 2010	Roving	Roving	Yes	Yes	Yes
EP3	19 February–16 March 2010	No	Fixed	Yes	No	Yes
IOP4	17–25 March 2010	Roving	Roving	Yes	Yes	Yes
EP4	26 March–8 April 2010	No	Fixed	Yes	No	Yes
IOP5	9–17 April 2010	Roving	Roving	Yes	Yes	Yes

[a] Intensive observing period.
[b] Extended observing period.

Table 3
RMSE for measured T_B based on cold (liquid nitrogen) and warm (microwave absorbing material) point calibration measurements, and estimated accuracy.

	6.9H	19 V	19H	37 V	37H	89 V	89H
Calibrations (n)	15	19	19	19	19	18	18
Cold point RMSE (K)	5.0	3.8	3.8	3.6	3.6	4.7	4.7
Warm pt. calibration RMSE (K)/	1.2	1.3	1.2	1.1	1.2	1.7	1.6
Estimated accuracy (K)	<2.0	<2.0	<2.0	<2.0	<2.0	<2.0	<2.0

specific surface area (SSA). This method does not provide a full three-dimensional visualization, and subjectivity is introduced by manually selecting the grains to be photographed and analyzed. However, these quantitative grain measurements provide an additional and unique measurement approach to manual snow grain size observations made with a field microscope. The enhanced protocol also included direct measurement of SSA using hemispheric laser-induced reflectance at 1300 nm following the technique described in Gallet et al. (2009). Due to the mechanics of sample removal from the snowpit, the vertical resolution of the laser measurements was approximately 5 cm.

In order to independently assess the seasonally evolving snow cover within each land cover type, 100 meter snow survey lines were established at each site, and surveyed weekly. For each survey, 201 depth measurements were made at 0.5 m spacing over a 100 m line. Bulk SWE and density were calculated from pairs of snow cores taken every 25 m along the sampling line. An ESC-30 snow corer (cross sectional area of 30 cm^2) was used for these measurements.

2.3. Brightness temperature simulations

Simulations of T_B were performed using the Helsinki University of Technology (HUT) snow emission model (Pulliainen et al., 1999) modified for multiple vertical layers as described in Lemmetyinen et al. (2010). Because this study includes experiments with the SWE retrieval scheme described in Pulliainen and Hallikainen (2001), which employs the HUT model as part of the SWE retrieval, we limited our perspective to this model. A full description of HUT model development and evaluation can be found in previous studies (Kontu & Pulliainen, 2010; Lemmetyinen et al., 2010; Pulliainen et al., 1999; Rees et al., 2010; Tedesco & Kim, 2006).

The first set of model simulations were performed for comparison with ground-based radiometer measurements at the forested, open fen, and lake sites, enabling a plot scale assessment of HUT model performance through the winter. Inputs to the model were derived from snowpit measurements: snow water equivalent, density, and grain size. Air and snow temperatures were measured at three nearby weather stations located in forest, open, and lakeshore environments. Simulations were run at each site with the snowpack optimized to 1 or 2 layers, and the surface roughness varied between 1 and 5 mm. After the November measurement period, the snowpack at each site contained more than 2 layers, so vertical simplification was required. Various characterizations of snow grain size were also utilized, as will be described in more detail in Section 3. The maximum number of snow layers was limited to 2 to not exceed the vertical snowpack complexity that could still be realistically applied in a daily, hemispheric, near real time implementation of the Pulliainen (2006) SWE retrieval scheme. For the lake ice site, one model layer was used for the ice, and the second for the overlying snow. The treatment of lake ice within the HUT model is described by Lemmetyinen et al. (2010), and further assessed by Gunn et al. (2011).

A second set of simulations were performed at the satellite scale for comparison with Advanced Microwave Scanning Radiometer (AMSR-E) measurements (Knowles et al., 2006). The proportional land cover for three categories (forest, open, lake) was determined from the National Topographic Data Base for Canada (see geogratis.cgdi.gc.ca) for a 3 by 3 EASE-Grid (Equal Area Scalable Earth Grid; 25 km resolution; see Armstrong & Brodzik, 1995) study area (Table 4). A single EASE-Grid cell encompassed all the ground measurement sites (Fig. 1). A scene simulation version of the HUT model was utilized for these model runs, which allowed separate treatment of the forest, open, and lake snowpacks, but computed an areal-weighted single top of atmosphere T_B at each grid cell for comparison with AMSR-E measurements. At the satellite scale, the effects of vegetation and the atmosphere are applied in the HUT model following Kruopis et al. (1999) and Pulliainen et al. (1999), respectively.

A SWE retrieval experiment using passive microwave (AMSR-E) measurements following the technique of Pulliainen et al. (1999) and Pulliainen and Hallikainen (2001) was also conducted for the study area shown in Fig. 1. This retrieval method is based on the minimization of the difference between satellite T_B measurements and simulations through a constrained least-squares algorithm in which the values for first grain size and then SWE are optimized. A single layer snowpack was used for the forward modeling components of the retrieval in order to match the current operational implementation of this retrieval method. Inputs to the forward T_B modeling component of the retrieval scheme were determined from the physical snow measurements made within the three land cover types throughout the 2009–2010 winter season.

3. Results

3.1. Snow evolution

Snow cover at the forest, open fen, and lake sites evolved uniquely through the winter season due to the different snow catchment and metamorphic processes that were predominant at each site. Time series of snowpack properties are shown in Fig. 3; measurement dates correspond to when radiometer measurements were also acquired at each site. The deepest snow occurred at the forest site – the open canopy coniferous forest is ideal for snow catchment with little redistribution by blowing snow. The density remained low (<0.250 g/cm^3) through the season. The development of large depth hoar at the base of the pack contributed to an increase in mean grain size through the season, with clearly defined rounded and recent snow layers at the top of the pack. The maximum snow depth at the fen site did not exceed approximately 30 cm – the height of the surface vegetation. Snow depth does not exceed the vegetation height due to redistribution during blowing snow events, as described in Pomeroy and Li (2000). This resulted in little change in snow depth during the coldest portion of the season, producing large depth hoar grains that eventually composed nearly 90% of the snowpack. The accumulation pattern at the lake site was solely the result of wind drifting. Snow depth remained shallow but dense, and the grains remained small, with little depth hoar.

3.2. Plot-scale simulations

Inputs to HUT snow emission model simulations were derived from snowpit observations: snow water equivalent, density, and grain size. Air and snow temperature were measured at three weather stations located in forest, open, and lakeshore environments. A series of simulations for the dates shown in Table 5 were run at each site with the snowpack

Table 4
Land cover composition for the grid cells shown in Fig. 1.

Grid	1	2	3	4	5	6	7	8	9
Open	0.16	0.62	0.62	0.14	0.46	0.77	0.32	0.21	0.43
Forest	0.62	0.27	0.27	0.76	0.26	0.08	0.17	0.06	0.10
Lake	0.22	0.11	0.11	0.10	0.28	0.15	0.51	0.73	0.48

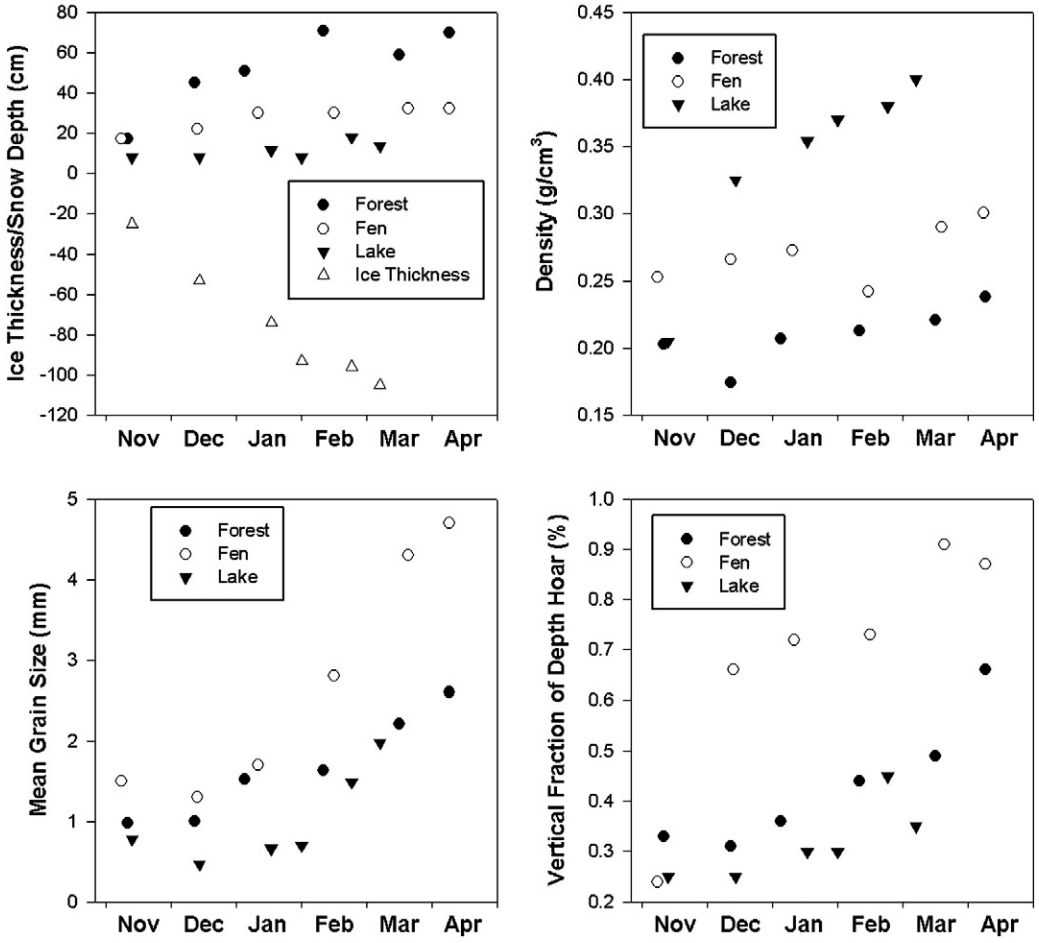

Fig. 3. Time series of snowpack properties at the forest, open fen, and lake sites. Mean grain size was determined from manual observations of grain axes dimensions. Ice thickness is considered from a datum of zero; negative numbers represent ice thickness from the surface.

optimized to 1 or 2 layers. For the 1 layer simulations, the bulk snowpack characteristics were derived through a vertically weighted average of the snow pit measurements. For the 2 layer simulations, vertically weighted averages based on proportional layer thicknesses were calculated for faceted grains (including depth hoar) and layers composed of new/recent and rounded grains. Emission from the ground/snow interface is determined with the semi-empirical model by Wegmüller and Mätzler (1999). The model introduces variability to the Fresnel reflection coefficients at V and H polarizations depending on the incidence angle and the effective surface roughness. Forward model iterations to determine the ideal surface roughness parameter were inconclusive, likely due to uncertainties introduced by manually clearing shallow snow from the footprint for the measurement of snow free T_B early in the campaign. The surface roughness was therefore varied between 1 and 5 mm, creating a small range in simulated T_B. For the initial set of model simulations, grain size was set using either the minimum or mean observations from the manual snowpits. For each site and time period, this created 20 total simulations due to the five rms values(1–5 mm), two grain characterizations (minimum and mean), and two layer configurations (1 and 2 layers).

Simulations were compared to the ground-based radiometer measurements; 19 and 37 GHz were the focus of this analysis as these frequencies are utilized within the SWE retrieval scheme assessed in Section 3.4. We avoided the use of a single measured T_B for evaluation of the simulations because of measurement variability introduced by radiometer calibration uncertainty and the measurement range from the multiple looks at overlapping footprints (as described in Section 2.1, the radiometers were shifted slightly for a sequence of measurements). This accounts for the range in measured T_B illustrated in Figs. 4, 6, 7, and 8; for the calculation of RMSE the mean measured T_B values were used.

Table 5
Radiometer measurement dates corresponding to plot scale T_B simulations.

Month	Forest	Fen	Lake
November	16 Nov. 2009	17 Nov. 2009	20 Nov. 2009
December	16 Dec. 2009	17 Dec. 2009	18 Dec. 2009
January	7 Jan. 2010	13 Jan. 2010	9 Jan. 2010
February	12 Feb. 2010	17 Feb. 2010	10 Feb. 2010
March	19 Mar. 2010	23 Mar. 2010	17 Mar. 2010
April	11 Apr. 2010	11 Apr. 2010	NA

3.2.1. Forest site

Two-layer simulation results for the forest site are shown in Fig. 4. For 19 GHz horizontal polarization (H-pol), the influence of ice lenses during March and April was the primary cause of an increased range in T_B measurements, and a higher uncertainty in simulated T_B as illustrated by the vertical lines in Fig. 4. An ice lens was not included as one of the snowpack layers, hence simulations overestimated T_B, consistent with the results of Rees et al. (2010). Because vertically polarized (V-pol) measurements are much less sensitive to ice layers, V-pol simulation uncertainty was much lower than at H-pol later in the season when ice lenses were present. At 37 GHz, the minimum grain size observations produced simulations that were too high; mean grain

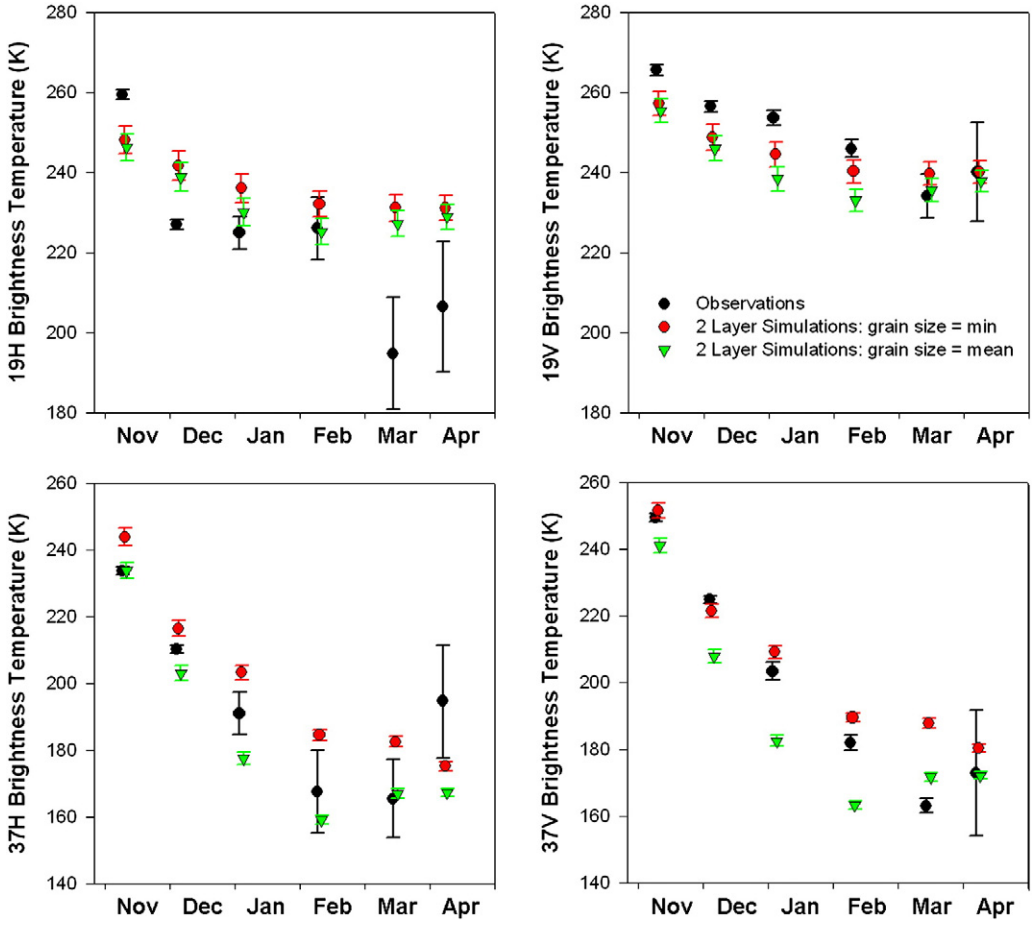

Fig. 4. Comparison of observed and 2-layer simulated T_B at the forest site using manual grain size observations.

sizes produced simulations that were too low. Reasonable 37 H-pol simulations using the mean grain size during March (when ice lenses were present) was a case of getting the right answer for the wrong reason: the larger grain size produced lower T_B's which matched the reduction in measured T_B due to the influence of the ice lenses (as described in Rees et al., 2010).

Ultimately, these results illustrate the unsatisfying subjective nature of using grain size determined from manual observations. However, additional grain size datasets acquired from January onwards provided a statistical characterization of grain size (with corresponding uncertainty) for the latter portion of the field campaign. The grain size datasets produced from the snowpit observations (minimum and mean), directional lighting photographs (long axis; short axis; SSA converted to grain size) and the laser SSA measurements (SSA converted to grain size) combined to produce 6 datasets from which the mean grain size and standard error were calculated:

$$SE = s\sqrt{n-1} \quad (1)$$

which depends on the standard deviation s of the n grain size datasets.

The plot-scale simulations at the forest site were re-run, using the mean multi-dataset grain size bounded by ± 1 SE as illustrated in Fig. 5. The results were very similar for both 1 layer and 2 layer representations of the snowpack (Fig. 6), suggesting the accurate field characterization of grain size for model input is more important than the number of layers in the simulations. These simulations also produced a more defensible solution due to the objective treatment of grain size compared to relying solely on manual snowpit observations. Statistically, the grain size standard error approach reduced the RMSE for 1 layer simulations by 2.8 and 9.1 K at 19H and 19 V, and 4.6 and 12.6 K at 37H and 37 V respectively.

3.2.2. Open wetland fen site

The snowpack evolution at the fen site produced very challenging conditions for plot scale model simulations. From January through April there was very little fresh snow accumulation, so grain size increased dramatically (because of a strong temperature gradient within the snowpack) with little to no increase in SWE. Results show that the model simulations were not able to account for the impact of this exceptional mid to late season grain growth (see Fig. 3), and T_B was progressively overestimated through the season (Fig. 7). By March, scattering by the snowpack is evident in the 19 GHz measurements, with very low T_B's at 37 GHz, particularly at H-pol, due to the combination of large grain size and ice lenses.

Improved treatment of grain size through the consideration of multiple datasets, as was successfully illustrated at the forest site, had little impact at the fen site. Model sensitivity runs showed that the impact of grain size reaches a threshold after which increased grain growth does not drive further reductions in simulated T_B (Fig. 8a) due to the scattering parameterization in the HUT model described by Kontu and Pulliainen (2010). This is problematic because the radiometer measurements at the fen site between January through April suggest that the growth of progressively larger grains does produce successively lower T_B's at both 19 and 37 GHz in the absence of any change in SWE. In cases where SWE increases coincident to grain growth (as occurred at the forest site) the model was able to simulate the very low T_B's measured in the field (as was shown in Fig. 7) because increases in SWE continue to drive simulated decreases in T_B with no maximum SWE threshold

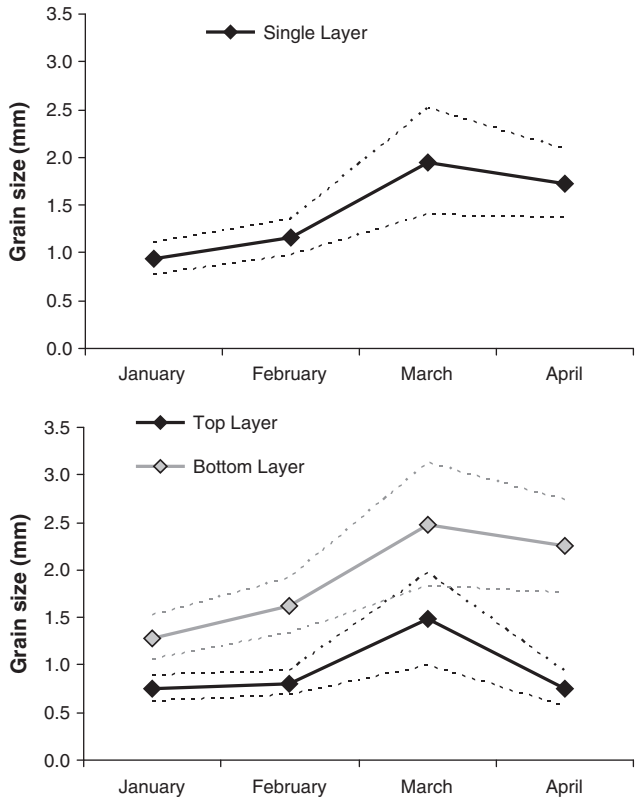

Fig. 5. Grain size (solid line) ±1 standard error (dashed line) for 1 and 2 layer representations of the forest snowpack.

(Fig. 8b). This is also somewhat problematic, however, because T_B at 37 GHz should not continue to decrease with increased SWE above approximately 150 mm due to the contribution of emission from the snowpack itself (Matzler, 1994; Matzler et al., 1982).

3.2.3. Lake site

Two-layer simulations were used at the lake site: one ice layer and one overlying snow layer. The snowpack over lake ice was relatively straightforward to characterize as a single layer because it remained shallow, dense, and primarily fine grained through the season (see Fig. 3). The observations and simulation results are shown in Fig. 9. At 19 GHz, the simulations were too high, but captured the increase in T_B through the season as ice thickness increased. A sensitivity analysis showed the simulated T_B is almost entirely influenced by ice thickness, with ice growth resulting in higher T_B (Fig. 10a and b), consistent with observations. Model performance at 37 GHz was more difficult to interpret because the measurements indicate sensitivity to ice growth (which acts to increase T_B) early in the season, and scattering from the snowpack (which acts to decrease T_B) later in the season. This complex temporal signature was illustrated through correlations between T_B and lake fraction at the satellite scale in Derksen et al. (2009). The sensitivity analysis, however, showed that the simulated T_B 37 GHz is entirely influenced by the snowpack (Fig. 10c and d); variability in ice thickness, even under thin ice conditions early in the season, had no impact on 37 GHz simulations.

3.2.4. Summary

The root mean square error (RMSE) for the 2-layer plot scale simulations using the mean observed grain size from the snowpit measurements are shown in Table 6. While other grain size treatments were utilized (as discussed previously) the mean snowpit measurement represents a consistent benchmark observation that was consistently acquired for all sites and all sampling periods. Simulations were averaged across the range of surface roughness values (1–5 mm), with the statistics calculated for (1) all cases, and (2) only those cases when the snowpack was free of ice lenses. Much lower uncertainty was produced at H-pol when no ice lenses were present at the forest and fen sites, an expected result due to the lack of an ice layer in the model configuration for all simulations.

3.3. Satellite-scale simulations

Land cover information from the National Topographic Data Base for Canada and forest biomass estimated from forest inventory information were compiled for a 3×3 study area of satellite passive microwave EASE-Grid (Equal Area Scaleable Earth Grid) cells (see Fig. 1). These sources of land cover information were then used for HUT model simulations that considered the sub-grid fractions of fen, forest, and lake cover. Snow inputs to the model (summarized in Table 7) were identical to those used in the plot scale simulations described previously but weighted by the fractional land cover of each grid cell (Table 4); mean manually observed grain size was used for all simulations (note that all the snow measurements occurred within grid cell 2, but were assumed to apply to the surrounding grid cells). The HUT model was configured to weight the simulations by the fractional land cover composition, allowing for direct comparison with satellite measurements. For this purpose, Advanced Microwave Scanning Radiometer (AMSR-E) T_B's were acquired from the National Snow and Ice Data Center (NSDIC).

A scatterplot of simulated versus observed T_B for grid cell 2 is shown in Fig. 11a. Observed T_B's were taken as a five-day moving average centered on the date of the snow measurements used as HUT model inputs. Model performance (Table 8) was improved compared to the plot scale results (Table 6), with RMSE ranging from 4 to 13 K depending on frequency and polarization. Additional uncertainty (RMSE ranging from 9 to 16 K)was introduced to the simulations for the other grid cells (Fig. 11b; Table 8) by using consistent snow characteristics for each land cover type as model inputs for all grid cells. In reality, there was likely meso-scale variability in snow and ice properties across the 3×3 grid cell (5625 km^2) study area. As shown in Table 8, agreement with the satellite observations across the larger study area (determined by RMSE) was slightly better at V-pol than H-pol; correlation results were significantly positive at 37 GHz, but weakly negative at 19 GHz. Although the RMSE was low, the poor correlation results at 19 GHz are due to the clustering of simulations evident in Fig. 11b. Grid cells 3 and 6 were not plotted in Fig. 11, or included in the statistics in Table 8 because the AMSR-E measurements clearly showed the influence of open water and sea ice introduced through the re-sampling of swath data into the EASE-Grid.

In summary, the RMSE values at the satellite scale were lower than at the plot scale. This is a positive result for operational implementation of the HUT model, and suggests that the impact of local scale parameters (such as grain size, density, depth hoar fraction, ice lenses) are clearly evident at the plot-scale and hence illustrate the model shortcomings. Statistical uncertainty was reduced when multiple snowpack types, land cover influences, and vegetation were integrated at the satellite scale, making model uncertainties less evident.

3.4. Satellite-scale SWE retrievals

A SWE retrieval experiment using passive microwave (AMSR-E) measurements was conducted for the Churchill area based on the technique of Pulliainen and Hallikainen (2001). Fig. 1 shows the 25 km resolution AMSR-E grid cells used for the retrievals; Table 4 summarizes the land cover fractions within each grid cell. The current implementation of the SWE retrieval technique uses a satellite scene

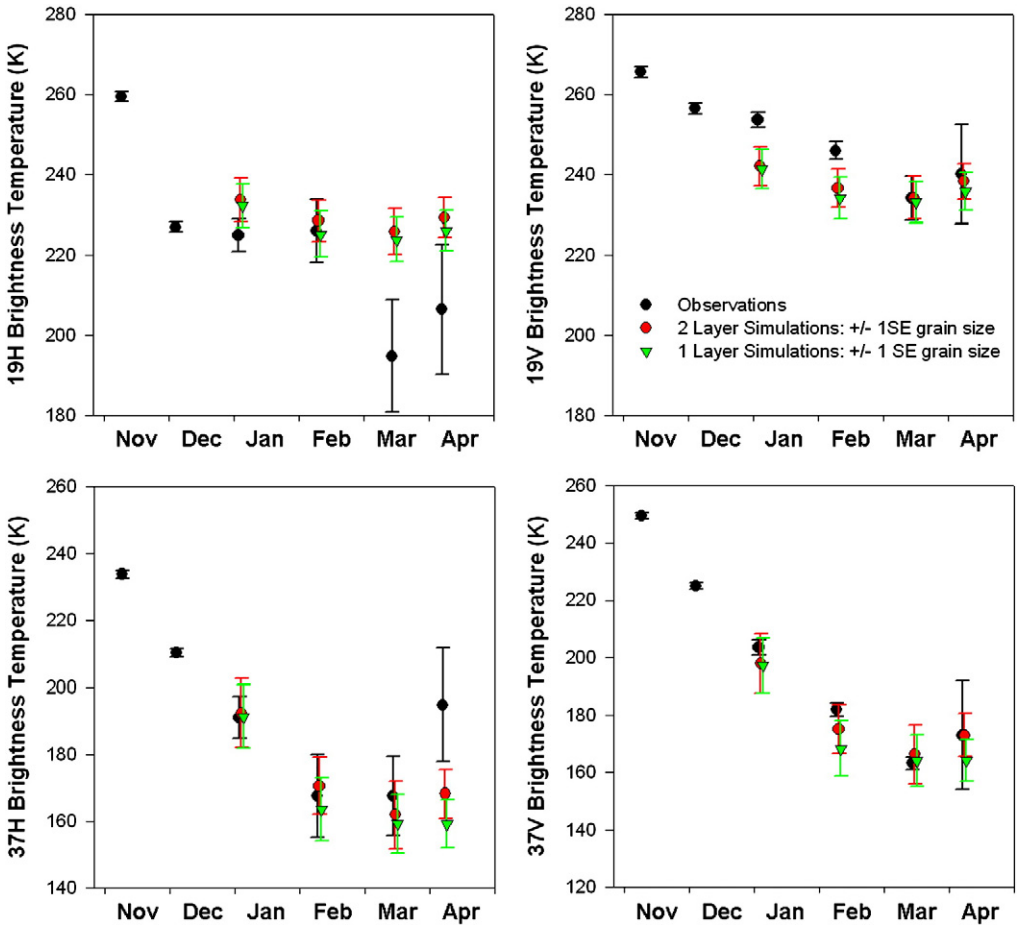

Fig. 6. Comparison of observed and simulated T_B at the forest site using the mean multi-dataset grain size bounded by ±1 standard error.

simulator developed at the Finnish Meteorological Institute (FMI) which allows for sub-grid cell segmentation by land cover. As with the satellite scale T_B simulations, three tiles (forest, open, lake) corresponding to the dominant cover types in the region were utilized. The same snow and vegetation data used as inputs to the satellite scale T_B simulations were used as inputs to the SWE retrieval scheme (see Table 7 for a summary of the retrieval model inputs). A single layer snowpack was used for the forward modeling components of the simulations.

A summary of the retrieval simulation results assessed against independent snow survey measurements is provided in Table 9. The 'ground truth' SWE was calculated by taking the landscape weighted average (forest; open; lake) from the weekly 100 m snow survey lines described in Section 2.1. Retrievals for grid cells 3 and 6 were again removed because of the influence of open water/sea ice on the AMSR-E measurements. It is evident that as lake ice fraction decreases, the accuracy of the retrievals improves. The results for grid cell 2 represent the best case scenario because the snow measurements used as model inputs were all made within this grid cell, and it contains low fractions of forest and lake cover, respectively. The assumption that these snow parameters are consistent across the study area introduces uncertainty into the snowpack characteristics used as model inputs, and for retrieval validation. Regional snow surveys conducted over 4 winter seasons and reported in Derksen (2008), however, suggest that changes in snow distribution and properties across the study domain are likely to be low.

The results in Table 9 are encouraging with respect to passive microwave SWE retrievals, however, this represents an ideal scenario in which snow cover characteristics were thoroughly measured through the complete winter season and available for input to the forward modeling component of the retrieval. In order to test retrieval performance under less idealized circumstances, the retrieval simulations were re-run with only a single land use tile. This better replicates an operational scenario where information from only a single snow survey or weather station would be available. Because these observations are often located in open areas (i.e. adjacent to airports) only the snow measurements from the open site were used as model inputs. Table 10 provides a summary of these retrievals; the accuracy is not influenced appreciably (and actually improved in some cases) compared to the simulations using the full set of snow observations. This suggests that snow information for a single land cover class can still result in useful retrievals.

4. Discussion and conclusions

The first objective of this study was to assess the ability of the HUT snow emission model to simulate T_B as compared to plot scale measurements made with ground based microwave radiometers at a network of sites. This fine scale approach is ideal for identifying the source of uncertainty in model simulations because the small size of the measurement footprint (~1 m by 1 m) can be precisely characterized by in-situ measurements. The simulation results showed that when grain size was relatively small (<2 mm) and no ice lenses were present, uncertainty was below 10 K. This represents strong model performance compared to other studies (see Kontu & Pulliainen, 2010; Lemmetyinen et al., 2010; Rees et al., 2010; Tedesco & Kim, 2006). When ice lenses were present, however, model performance reduced appreciably at H-pol. The proper treatment of ice lenses requires a layer in the snow emission model dedicated to an ice lens when appropriate. This creates an implementation issue

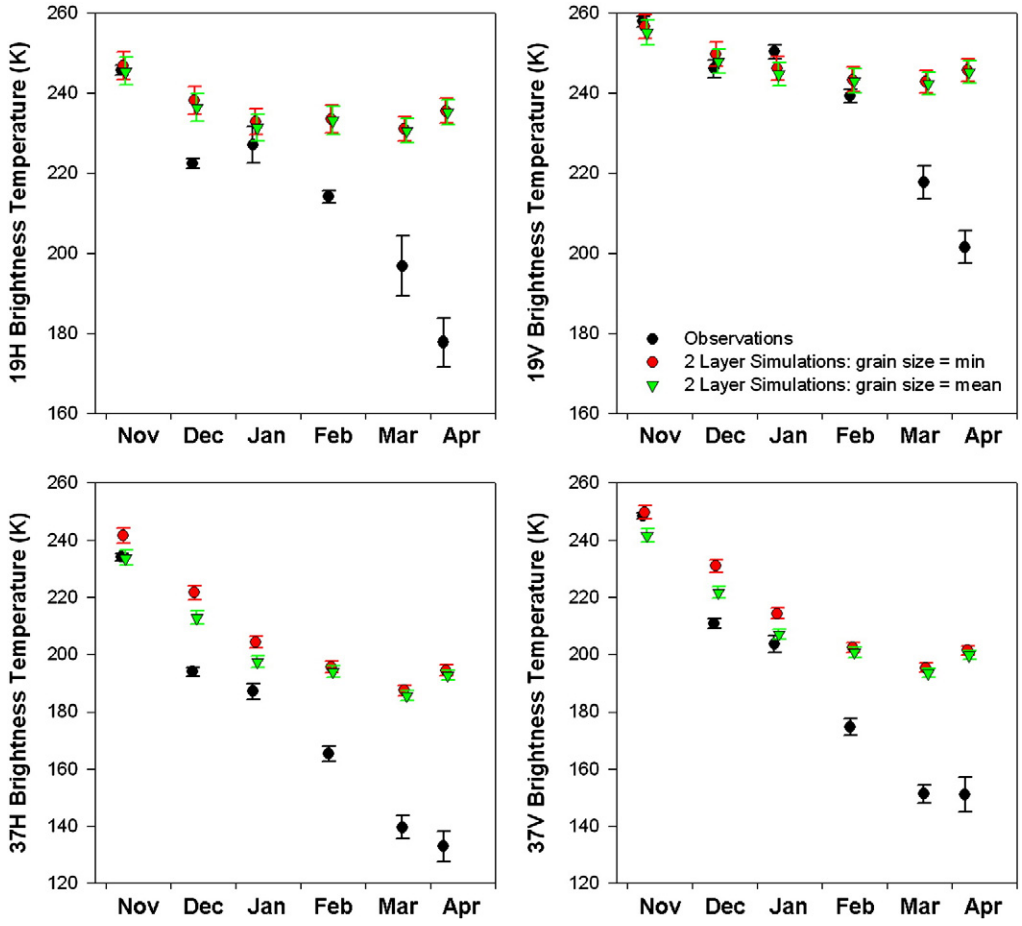

Fig. 7. Comparison of observed and 2-layer simulated T_B at the fen site using manual grain size observations.

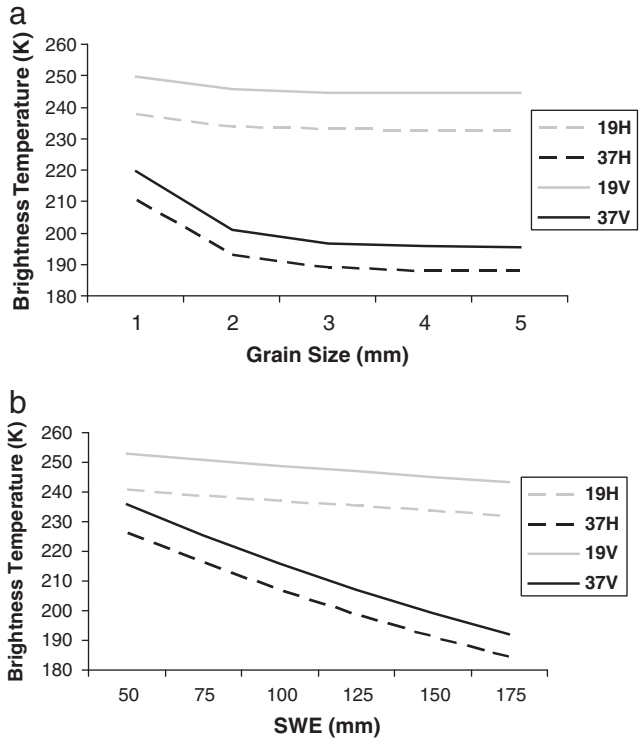

Fig. 8. Simulated T_B with the HUT model with (a) varying grain size (SWE = 90; density = 0.275; rms = 3; $T_{air} = -10$; $T_{snow} = -5$; $T_{ground} = -3$); (b) varying SWE (density = 0.275; grain size = 1; rms = 3; $T_{air} = -10$; $T_{snow} = -5$; $T_{ground} = -3$).

because only a single snow layer is currently employed for forward T_B simulations at hemispheric/global scales (for example, in the GlobSnow SWE product) due to difficulties in segmenting the snowpack into multiple layers from operationally available snow observations. It would be feasible, however, to test for the presence of ice lenses using satellite passive microwave polarization ratio thresholds (as illustrated by Derksen et al., 2009; Grenfell & Putkonen, 2008) and adding an ice lens layer should one be detected.

The second objective of the study was to compare simulations at the satellite scale to measurements from the Advanced Microwave Scanning Radiometer (AMSR-E). The predominant issues at the plot scale (large grain size; ice lenses) were less evident at the satellite scale – uncertainty was reduced when the three predominant land cover types were integrated into a single simulation.

The final objective was to assess a SWE retrieval scheme based on Pulliainen et al. (1999) using the snowpack measurements acquired through an observation rich season combined with AMSR-E data. Results were particularly sensitive to the grid cell lake fraction: RMSE of the retrievals ranged from 20 to over 70 mm when the results were segmented by lake fraction. The coarse resolution of the AMSR-E measurements is also a limiting factor because a single retrieval is produced for grid cells that contain an implicitly high level of heterogeneity. Fig. 12 shows the range of SWE measured from the 100 meter snow surveys across the land cover types. The passive microwave retrieval provides a single value that falls at variable points within these sub-grid ranges. High resolution measurements, for instance using Ku- and X-band radar as proposed in the ESA CoReH20 mission (Rott et al., 2009), have the potential to better resolve this heterogeneity.

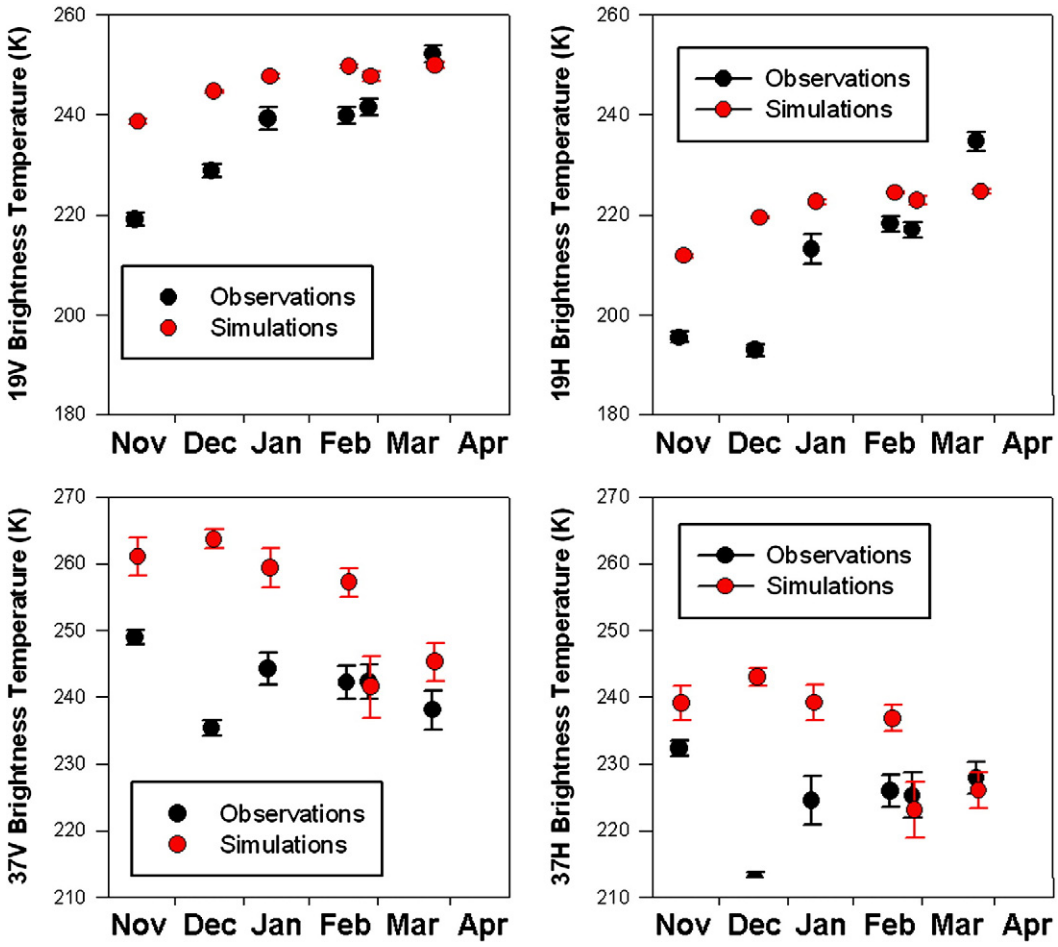

Fig. 9. Comparison of observed and simulated T_B at the lake site using manual grain size observations.

The following sources of uncertainty identified in this study require further attention:

Lake fraction: The retrieval model allows the land surface to be tiled into fractions with unique snow cover properties. For this experiment, three predominant land cover categories were utilized: forest, open, and lakes. Retrieval uncertainty increased with lake fraction; beyond a threshold of 50% the retrievals had no relationship with reference SWE measurements. The HUT emission model for lake ice assumes the ice to be a non-scattering layer with the absorptive properties of pure ice. Lake ice cores extracted during the 2009–2010 winter season near Churchill, however, showed frequent occurrence of white ice (snow ice, or superimposed ice), spherical bubble rich layers near the snow/ice interface, and elongated bubbles near the water/ice interface, consistent with measurements made at other sub-Arctic lakes (Gunn et al., 2011).

Sensitivity to grain size: Snow emission models are highly sensitive to the treatment of grain size, yet this variable is exceptionally difficult to measure quantitatively in the field. Considerable effort was spent on quantitative grain size measurement during the 2009–2010 Churchill campaign, including (1) conventional estimates using a field microscope, (2) near infrared photography following Langlois et al. (2010), (3) 2-D grain morphology from crystal photography, and (4) laser-induced reflectance measurements following Gallet et al. (2009). These measurement techniques produced a range of grain sizes for forward T_B modeling and SWE retrieval inputs. This wealth of information is still difficult to apply in a modeling context because snow is a layered medium that must be simplified to one or two layers for modeling applications. This vertical simplification of the snowpack introduces uncertainty. Even within snowpack layers, grain sizes are not uniform, but occur across a distribution, which is problematic for models like HUT which require a single grain size value for each layer. Statistical characterization from multiple observational datasets of a mean grain size ± 1 SE reduced simulation RMSE errors at the forest site, and better represents the non-uniformity of naturally occurring grain size both within individual layers and within the integrated snow volume. Simulations across this range of observed grain sizes results in a broad distribution of simulated T_B (see Fig. 6) which introduces further challenges for model application and interpretation. Additionally, considerable time is required to collect this range of grain size measurements in the field. At the fen and lake sites, the additional grain size datasets did not improve model performance because of issues related to the model parameterization of large grains, and lake ice respectively.

The SWE retrieval simulations showed that good results were achieved when using the mean grain size measurement available from manual field observations, but more work is necessary to quantify grain size in the most objective way possible under field conditions, and use this information in a meaningful way for modeling applications. Another approach is to utilize the HUT model to derive effective grain size as a retrieval output, which could then be compared to the measured values.

Dependence on high quality snow observations: This SWE retrieval experiment represented a 'best-case scenario' because the study area was observation rich. Detailed snowpack measurements were available for all land cover types through the complete winter

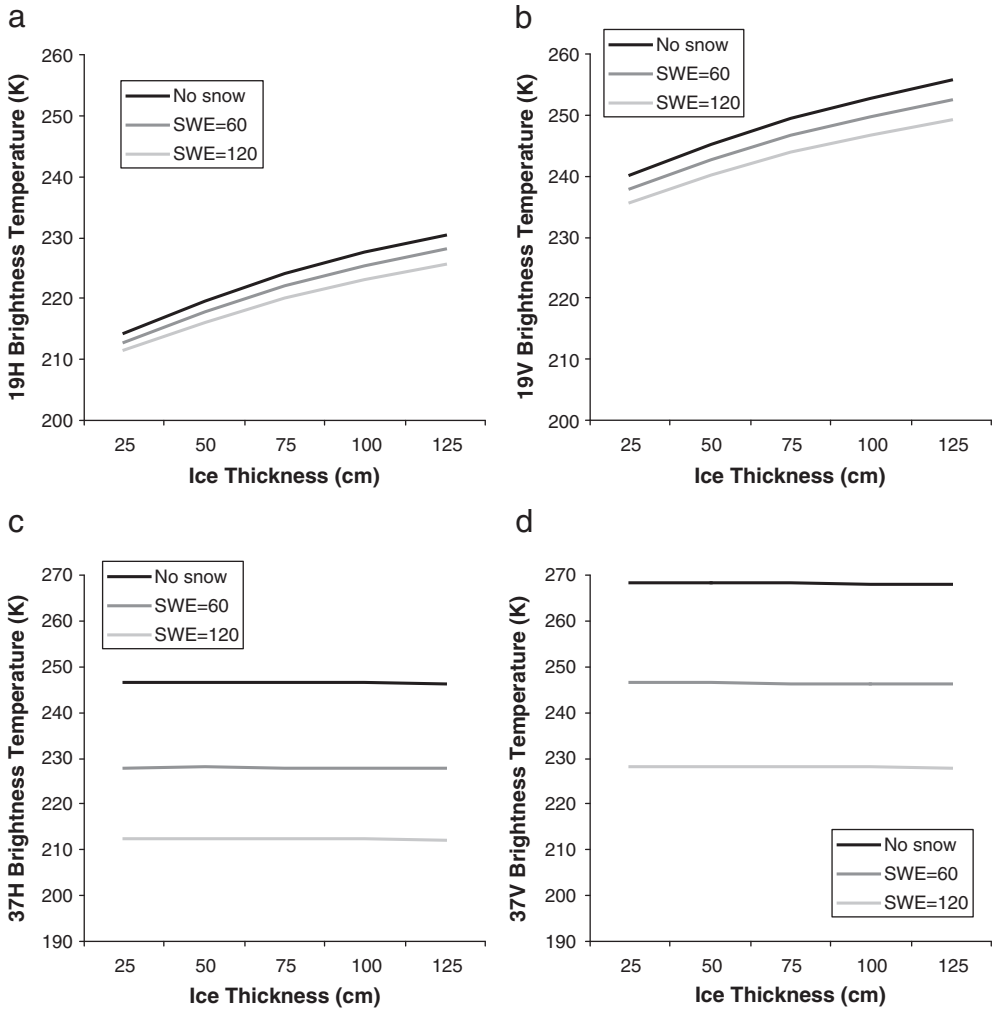

Fig. 10. Simulated T_B with the HUT model with varying ice thickness and SWE (density = 0.350; rms = 1; $T_{air} = -10$; $T_{snow} = -5$; $T_{ice} = -3$; $T_{water} = 0$).

season. This allowed the model simulations to be configured based on high quality observations. In an operational context, it is typical to only know snow depth for a single point, with large distances between these observations. It is therefore necessary to infer information on variables such as snow density and grain size, either from climatology, a physical snow model (i.e. Langlois et al., 2009), or some other stochastic approach. This lack of observations introduces uncertainty in model inputs. While generalizing the snow information did not appreciably reduce the quality of the SWE retrievals in this study, the assumption of consistent snow properties across the meso-scale study area will become more problematic as the study area is increased.

The datasets acquired during the 2009–2010 field campaign near Churchill, Manitoba represent a unique observational time series of snow physical properties coupled with passive microwave measurements. Field observations of passive microwave T_B are

Table 6
RMSE (K) for plot scale simulated (2 layers; mean observed grain size) versus measured T_B.

All cases	Forest	Fen	Lake
n	30	30	25
19H	17.8	28.9	17.6
19V	10.2	20.7	14.3
37H	13.2	34.2	12.1
37V	14.2	23.0	10.1
No lenses	**Forest**	**Fen**	**Lake**
N	10	10	5
19H	9.3	12.0	14.3
19V	12.4	3.8	12.7
37H	8.7	18.0	12.8
37V	16.9	14.7	11.4

Table 7
Configuration for satellite scale T_B simulations and SWE retrieval experiments.

Depth (cm)	Nov	Dec	Jan	Feb	Mar	Apr
Open	17	22	31	33	34	30
Forest	21	45	51	71	59	69
Lake	8	8	12	18	14	14
Density (g/cm^3)	**Nov**	**Dec**	**Jan**	**Feb**	**Mar**	**Apr**
Open	0.253	0.266	0.273	0.242	0.290	0.300
Forest	0.233	0.174	0.207	0.213	0.221	0.238
Lake	0.205	0.325	0.354	0.380	0.400	0.400
Mean grain size (mm)	0.9	1.0	1.3	1.9	2.9	3.4
Roughness (mm)	3	3	3	3	3	3
Permittivity (F/m)	6-1*j	6-1*j	6-1*j	6-1*j	6-1*j	6-1*j
Biomass volume (m^2/ha)	70	70	70	70	70	70

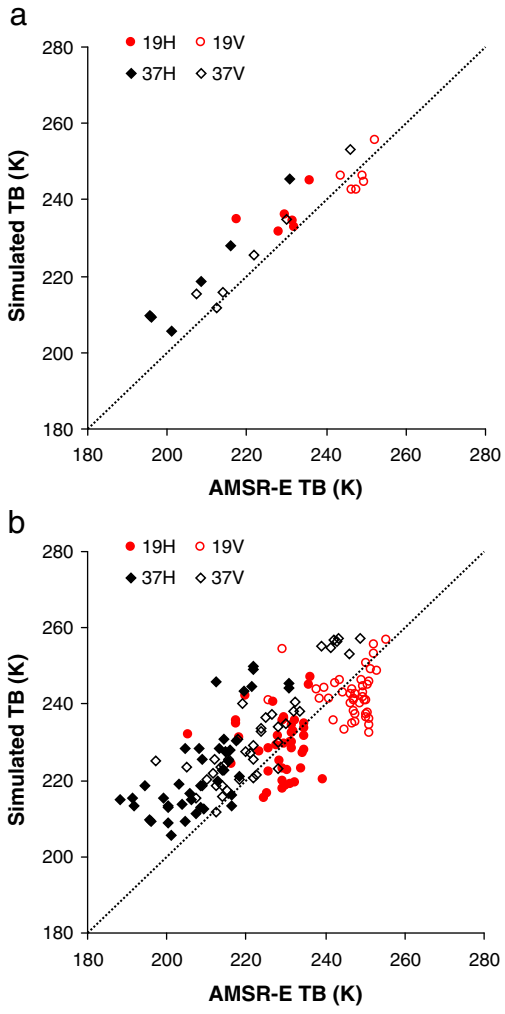

Fig. 11. Simulated versus observed T_B for (a) grid cell 2; and (b) all grid cells with the exception of 3 and 6.

Table 9
Summary of SWE retrieval results.

d_o = mean	r	RMSE (mm)	Bias (mm)
All cases	0.34	75	−59
Lake<50	0.48	56	−35
Lake<25	0.53	55	−28
Grid 2	0.94	22	−20

Table 10
Summary of SWE retrieval results using simplified snow inputs.

d_o = mean	r	RMSE (mm)	Bias (mm)
All cases	0.35	63	−49
Lake<50	0.46	53	−32
Lake<25	0.51	52	−25
Grid 2	0.95	22	−20

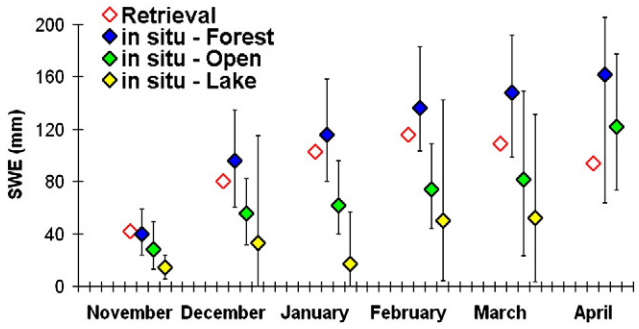

Fig. 12. Solid symbols show mean measured SWE- along 100 m snow surveys for lake, forest, and open environments; vertical lines illustrate maximum and minimum measurements. Red symbols show passive microwave retrieved SWE for each month.

typically acquired at discrete time periods within a winter season. For example, ground based radiometer measurements acquired during the Cold Land Processes Experiment (CLPX) conducted during 2002 and 2003 in Colorado were limited to only a 2 week period (Cline et al., 2003). Still, these observations have been widely used to investigate the performance of snow emission models (i.e. Durand et al., 2008; Tedesco & Kim, 2006) and SWE retrieval techniques (i.e. Durand et al., 2009). The seasonal perspective of the 2009, 2010 Churchill campaign enhances our ability to assess snow emission models and SWE retrieval techniques through the evolution of a single layer, fine grained snow cover to a vertically complex and layered medium. Passive microwave observations are presently being combined with the Ku- and X-band scatterometer measurements also acquired during the campaign to address the synergistic (active and passive microwave) retrieval of SWE, relevant to the proposed ESA CoReH20 mission.

Acknowledgments

The 2009–2010 field measurement campaign in Churchill was supported by the Canadian Space Agency and Environment Canada. Thanks to Arvids Silis, Josh King, Grant Gunn, Kevin Kang, Claude Duguay, Richard Kelly, Alain Royer, Andrew Rees, Walter Strapp, and Ken Asmus for their contributions to the field program. Logistical support in the field was provided by the Churchill Northern Studies Centre (thanks to LeeAnn Fishback, Carley Basler, and Clifford Paddock). Thanks to Alexandre Roy and Benoit Montpetit for provision of grain size and SSA measurements. Helpful comments on an earlier version of this manuscript were provided by Michael Kern (European Space

Table 8
Summary of Pearson correlation and RMSE statistics, simulated versus AMSR-E T_B. Significant correlations at 95% are in bold italics.

	19H		19 V		37H		37 V	
	RMSE	Correlation	RMSE	Correlation	RMSE	Correlation	RMSE	Correlation
Grid 2	5.9	0.44	3.8	***0.65***	12.8	***0.97***	6.1	***0.98***
All cases	10.0	−0.01	9.3	0.03	16.0	***0.74***	10.5	***0.88***

Agency). AMSR-E brightness temperature data were acquired from the National Snow and Ice Data Center in Boulder.

References

Armstrong, R., & Brodzik, M. (1995). An earth-gridded SSM/I data set for cryospheric studies and global change monitoring. *Advanced Space Research*, *16*(10), 10155–10163.

Armstrong, R., & Brodzik, M. (2002). Hemispheric-scale comparison and evaluation of passive-microwave snow algorithms. *Annals of Glaciology*, *34*, 38–44.

Brasnett, B. (1999). A global analysis of snow depth for numerical weather prediction. *Journal of Applied Meteorology*, *38*, 726–740.

Brown, R., Derksen, C., & Wang, L. (2010). A multi-dataset analysis of variability and change in Arctic spring snow cover extent, 1967–2008. *Journal of Geophysical Research*, *115*, D16111, doi:10.1029/2010JD013975.

Brown, R., & Robinson, D. (2011). Northern Hemisphere spring snow cover variability and change over 1922–2010 including an assessment of uncertainty. *The Cryosphere*, *5*, 219–229.

Carroll, T., Cline, D., Olheiser, C., Rost, A., Nilsonn, A., Fall, G., et al. (2006). NOAA's national snow analysis. *Proceedings, 74th western snow conference*.

Cline, D., Elder, K., Davis, B., Hardy, J., Liston, G., Imel, D., et al. (2003). Overview of the NASA cold land processed field experiment (CLPX-2002). In C. Kummerow, J. Jiang, & S. Uratuka (Eds.), *Microwave remote sensing of the atmosphere and environment III. Proceedings of SPIE*, *Vol. 4894*. (pp. 361–372).

Colbeck, S., Akitaya, E., Armstrong, R., Gubler, H., Lafeuille, J., Lied, K., et al. (1992). *The international classification for seasonal snow on the ground*. The International Commission on Snow and Ice of the International Association of Scientific Hydrology/International Glaciological Society/U.S. Army CRREL Report (37 pp.).

Derksen, C. (2008). The contribution of AMSR-E 18.7 and 10.7 GHz measurements to improved boreal forest snow water equivalent retrievals. *Remote Sensing of Environment*, *112*, 2700–2709.

Derksen, C., Sturm, M., Liston, G., Holmgren, J., Huntington, H., Silis, A., et al. (2009). Northwest Territories and Nunavut snow characteristics from a sub-Arctic traverse: Implications for passive microwave remote sensing. *Journal of Hydrometeorology*, *10*(2), 448–463.

Durand, M., Kim, E., & Margulis, S. (2008). Quantifying uncertainty in modeling snow microwave radiance for a mountain snowpack at the point scale, including stratigraphic effects. *IEEE Transactions on Geoscience and Remote Sensing*, *46*(6), 1753–1767.

Durand, M., Kim, E., & Margulis, S. (2009). Radiance assimilation shows promise for snowpack characterization. *Geophysical Research Letters*, *36*, L02503, doi:10.1029/2008GL035214.

Foster, J. A., & Chang, D. Hall (1997). Comparison of snow mass estimates from a prototype passive microwave snow algorithm, a revised algorithm and a snow depth climatology. *Remote Sensing of Environment*, *62*, 132–142.

Gallet, J. -C., Domine, F., Zender, C., & Picard, G. (2009). Measurement of the specific surface area of snow using infrared reflectance in an integrating sphere at 1310 and 1550 nm. *The Cryosphere*, *3*, 167–182.

Grenfell, T., & Putkonen, J. (2008). A method for the detection of the severe rain-on-snow event on Banks Island, October 2003, using passive microwave remote sensing. *Water Resources Research*, *44*, W03425, doi:10.1029/2007SR005929.

Gunn, G., Duguay, C., Derksen, C., Lemmetyinen, J., & Toose, P. (2011). Evaluation of the Helsinki University of Technology's modified snow emission model over lake ice using airborne passive microwave measurements. *Remote Sensing of Environment*, *115*, 233–244.

Jonas, T., Marty, C., & Magnusson, J. (2009). Estimating the snow water equivalent from snow depth measurements in the Swiss Alps. *Journal of Hydrology*, *378*, 161–167.

Kelly, R. (2009). The AMSR-E snow depth algorithm: Description and initial results. *Journal of The Remote Sensing Society of Japan*, *29*, 307–317.

Kelly, R., Chang, A., Tsang, L., & Foster, J. (2003). A prototype AMSR-E global snow area and snow depth algorithm. *IEEE Transactions on Geoscience and Remote Sensing*, *41*(2), 230–242.

Knowles, K. W., Savoie, M. H., Armstrong, R. L., & Brodzik, M. J. (2006). *Updated 2010*. AMSR-E/Aqua daily EASE-Grid brightness temperatures, 2002–2008. Boulder, Colorado USA: National Snow and Ice Data Center. Digital media.

Koenig, L., & Forster, R. (2004). Evaluation of passive microwave snow water equivalent algorithms in the depth hoar-dominated snowpack of the Kuparuk River watershed, Alaska, USA. *Remote Sensing of Environment*, *93*, 511–527.

Kontu, A., & Pulliainen, J. (2010). Simulation of spaceborne microwave radiometer measurements of snow cover using in situ data and brightness temperature modeling. *IEEE Transactions on Geoscience and Remote Sensing*, *48*, 1031–1044.

Kruopis, N., Praks, J., Arslan, A., Alasalmi, H., Koskinen, J., & Hallikainen, M. (1999). Passive microwave measurements of snow-covered forest areas in EMAC'95. *IEEE Transactions on Geoscience and Remote Sensing*, *37*(6), 2699–2705.

Langlois, A., Brucker, L., Kohn, J., Royer, A., Derksen, C., Cliche, P., et al. (2009). Simulation of snow water equivalent (SWE) using thermodynamic snow models in Québec, Canada. *Journal of Hydrometeorology*, *10*, 1447–1462.

Langlois, A., Royer, A., Montpetit, B., Picard, G., Brucker, L., Arnaud, L., et al. (2010). On the relationship between snow grain morphology and in-situ near infrared calibrated reflectance photographs. *Cold Regions Science and Technology*, *61*, 34–42.

Lemmetyinen, J., Pulliainen, J., Rees, A., Kontu, A., Qiu, Y., & Derksen, C. (2010). Multiple layer adaptation of the HUT snow emission model: Comparison with experimental data. *IEEE Transactions on Geoscience and Remote Sensing*, *48*, 2781–2794.

Matzler, C. (1994). Passive microwave signatures of landscapes in winter. *Meteorology and Atmospheric Physics*, *54*, 241–260.

Matzler, C., Schanda, E., & Good, W. (1982). Towards the definition of optimum sensor specifications for microwave remote sensing of snow. *IEEE Transactions on Geoscience and Remote Sensing. GE-20*. (pp. 57–66).

Pomeroy, J., & Li, L. (2000). Prairie and Arctic areal snow cover mass balance using a blowing snow model. *Journal of Geophysical Research*, *105*(D21), 26619–26634.

Pulliainen, J. (2006). Mapping of snow water equivalent and snow depth in boreal and sub-arctic zones by assimilating space-borne microwave radiometer data and ground-based observations. *Remote Sensing of Environment*, *101*(2), 257–269.

Pulliainen, J., Grandell, J., & Hallikainen, M. (1999). HUT snow emission model and its applicability to snow water equivalent retrieval. *IEEE Transactions on Geoscience and Remote Sensing*, *37*(3), 1378–1390.

Pulliainen, J., & Hallikainen, M. (2001). Retrieval of regional snow water equivalent from space-borne passive microwave observations. *Remote Sensing of Environment*, *75*, 76–85.

Rees, A., Lemmetyinen, J., Derksen, C., Pulliainen, J., & English, M. (2010). Observed and modelled effects of ice lens formation on passive microwave brightness temperatures over snow covered tundra. *Remote Sensing of Environment*, *114*, 116–126.

Rott, H., Duguay, C., Essery, R., Haas, C., Macelloni, G., Malnes, E., et al. (2009). *ESA SP-1313/3 candidate earth explorer core missions report for assessment: CoReH20 – Cold regions hydrology high resolution observatory* (pp. 114). : ESA Communication Production Office.

Rutter, N., Cline, D., & Li, L. (2008). Evaluation of the NOHRSC snow model (NSM) in a one-dimensional mode. *Journal of Hydrometeorology*, *9*, 695–711.

Solheim, F. 1993. Use of pointed water vapor radiometer observations to improve vertical GPS surveying accuracy, Ph.D. dissertation, Dept. Physics, Univ. Colorado, Boulder, 1993.

Sturm, M., Taras, B., Liston, G., Derksen, C., Jonas, T., & Lea, J. (2010). Estimating snow water equivalent using snow depth data and climate classes. *Journal of Hydrometeorology*, *11*, 1380–1394.

Takala, M., Luojus, K., Pulliainen, J., Derksen, C., Lemmetyinen, J., Kärnä, J. -P., Koskinen, J., & Bojkov, B. (2011). Estimating northern hemisphere snow water equivalent for climate research through assimilation of space-borne radiometer data and ground-based measurements. *Remote Sensing of Environment*, doi:10.1016/j.rse.2011.08.014.

Tedesco, M., & Kim, E. (2006). Intercomparison of electromagnetic models for passive microwave remote sensing of snow. *IEEE Transactions on Geoscience and Remote Sensing*, *44*(10), 2654–2666.

Wegmüller, U., & Mätzler, C. (1999). Rough bare soil reflectivity model. *IEEE Transactions on Geoscience and Remote Sensing*, *37*, 1391–1395.

Wiesmann, A., & Matzler, C. (1999). Microwave emission model of layered snowpacks. *Remote Sensing of Environment*, *70*, 307–316.